QUARTERLY JOURNAL OF THE ROYAL METEOROLOGICAL SOCIETY
RMetS Royal Meteorological Society

The role of atmospheric uncertainty in Arctic sea ice data assimilation and prediction

Journal:	*QJRMS*
Manuscript ID:	Draft
Wiley - Manuscript type:	Research Article
Date Submitted by the Author:	n/a
Complete List of Authors:	Yang, Qinghua; Alfred Wegener Institute, ; National Marine Environmental Forecasting Center, Losa, Svetlana; Alfred Wegener Institute, Losch, Martin; Alfred Wegener Institute, Jung, Thomas; Alfred Wegener Institute, Nerger, Lars; Alfred Wegener Institute,
Keywords:	TIGGE, sea ice, Arctic, data assimilation, ensemble Kalman filter, ensemble forecast

The role of atmospheric uncertainty in Arctic sea ice data assimilation and prediction

Qinghua Yang[1,2], Svetlana N. Losa[2], Martin Losch[2], Thomas Jung[2], Lars Nerger[2]

1. Polar Environmental Research and Forecasting Division, National Marine Environmental Forecasting Center, Beijing, China
2. Alfred Wegener Institute, Helmholtz Centre for Polar and Marine Research, Bremerhaven, Germany

Correspondence to: Q. Yang, National Marine Environmental Forecasting Center, Rd. Dahuisi 8, Beijing, China. E-mail: Qinghua.Yang@awi.de

The role of atmospheric uncertainty for the assimilation and prediction of Arctic sea ice is explored by running the Massachusetts Institute of Technology general circulation model (MITgcm) in data assimilation and prediction mode for the summer 2010. The atmospheric ensemble forcing is taken from the UK Met Office (UKMO) system available through the TIGGE (THORPEX Interactive Grand Global Ensemble) database. The DA system is based on a local Singular Evolutive Interpolated Kalman (LSEIK) filter and Special Sensor Microwave Imager/Sounder (SSMIS) sea ice concentration operational products from the National Snow and Ice Data Center (NSIDC) are assimilated. Two kinds of experiments are carried out differing in the LSEIK configuration and forcing used: The first one uses a single deterministic control forcing and a forgetting factor necessary to inflate the ensemble spread in the DA phase; the second one uses 23 members from the UKMO atmospheric ensemble prediction system without additional ensemble inflation. The latter configuration is more straightforward to implement since the atmospheric ensemble forcing explicitly accounts for model errors making additional tuning obsolete. Comparisons with sea ice observation data show that both systems improve the analyzed and 24-h forecasted sea ice concentration and thickness. However, ice concentration is better represented with the new ensemble forcing approach. Using ensemble forcing can also improve 15-day ice concentration forecasts that are initialized from the first assimilation experiment with single control forcing.

Key Words: TIGGE; sea ice; Arctic; data assimilation; ensemble Kalman filter; ensemble forecast

1. Introduction

Satellite observations show Arctic sea ice extent and volume consistently decreased in all seasons for the past 30 years, with a maximum decline in summer (IPCC, 2013). According to the latest climate model predictions, the Arctic Ocean will become ice-free by the middle of 21th century in high emission scenarios (Liu et al., 2013). The decrease of summer sea ice extent opens new shipping routes in the Arctic Ocean and creates the potential for a wide range of economic activities. In order to thoroughly manage the opportunities and risks associated with Arctic sea ice decline accurate sea ice forecasts are required (e.g. to ensure marine safety, Eicken, 2013).

There are several factors that can affect the sea ice forecasting behavior, e.g., the systematic biases in the model configuration or atmospheric forcing, and the data assimilation techniques (Yang et al., 2014). In general, sea ice concentration forecasts can be improved by data assimilation (Lisæter et al., 2003; Lindsay and Zhang,2006; Stark et al., 2008; Sakov et al., 2012; Tietsche et al., 2013; Buehner et al., 2013; and Yang et al., 2014). In most previous studies sea ice-ocean models are driven by single deterministic atmospheric forcing fields; and by doing so uncertainties and biases in the forcing are neglected (Park et al., 2008). Still there are several methods to accounting for possible uncertainties in external forcing. Sakov et al. (2012), for example, considered the model error by increasing the model spread through perturbation of a number of forcing fields; and Yang et al. (2014) inflated the forecast error covariance with a so-called forgetting factor (Pham, 2001). However, to the authors' knowledge, this is the first study on Arctic sea ice data assimilation and prediction in which realistic, flow-dependent atmospheric uncertainty is taken into account.

Atmospheric Ensemble prediction systems (EPS) have evolved substantially since their first appearance in the 1990s (e.g. Jung and Leutbecher, 2007), they are now widely used to represent the effect of observation uncertainties, atmospheric model uncertainties, imperfect boundary conditions and data assimilation assumptions in weather forecasting (Park et al., 2008). The availability of global EPSs from 10 leading operational centers through the 'THORPEX Interactive Grand Global Ensemble' (TIGGE) (Park et al., 2008; Bougeault et al., 2010) offers a new opportunity for the design of Arctic sea ice ensemble forecasting systems.

In this study, model uncertainties are represented by using a subset of the TIGGE ensemble atmospheric forecasting data, its influences on both sea ice data assimilation and forecasts are examined. In particular, we investigate: 1) whether the atmospheric ensemble implementation allows to sufficiently well approximate the sea ice model error statistics and, therefore, to improve the system state estimation/initialization and short-term forecast; 2) whether the ensemble of atmospheric conditions leads to more reliable sea ice medium-range forecasts. To answer these questions, following Yang et al. (2014), a local ensemble-based Singular Evolutive Interpolated Kalman (SEIK) filter (Pham et al., 1998; Pham, 2001) is used to assimilate sea ice concentration into Massachusetts Institute of Technology general circulation model (MITgcm;Marshall et al., 1997) over a summer period of 3 months in summer 2010. The effectiveness of the ensemble forcing is analyzed by comparing with the 24-h and 15-day sea ice forecasts using TIGGE control forcing, and the sea ice concentration and thickness observations.

2. Forecasting System

2.1 MITgcm ice-ocean model

The model used in this study is the MITgcm sea ice-ocean model. It includes state-of-the-art sea-ice dynamics based on Zhang and Hibler III (1997) and simple zero-layer thermodynamics (Losch et al., 2010). Following Losch et al. (2010) and Nguyen et al. (2011), we employ an Arctic regional configuration with open boundaries in both the Atlantic and Pacific sectors. Monthly ocean boundary conditions are provided from a global configuration (Menemenlis et al., 2008). The horizontal domain grid is locally orthogonal and has an average spacing of 18 km. The same

horizontal mesh is used to solve the ocean and sea ice equations. The vertical resolution is highest in the upper ocean, with 28 vertical levels in the top 1000 m and additional 22 layers below 1000m. Bathymetry is derived from the U.S. National Geophysical Data Center (NGDC) two-minute global relief dataset (ETOPO2; Smith and Sandwell, 1997). The monthly mean river runoff is based on the Arctic Runoff Data Base (ARDB) (see Nguyen et al., 2011 for more details).

2.2 UKMO forcing data from TIGGE archive

We use atmospheric ensemble forecasts of the UK Met Office (UKMO) available in the TIGGE archive (http://tigge.ecmwf.int/). The UKMO EPS uses an Ensemble Transform Kalman Filter (ETKF; Bishop et al., 2001) and the Shutts (2005) scheme to simulate initial uncertainties and the effect of model uncertainties, respectively (Bowler et al., 2007). It has a very good forecasting quality (Park et al., 2008). The number of ensemble members available from the UKMO EPS (23) can easily be used for an approximation of the forecast error statistics in our sea ice data assimilation system based on reduced rank filtering (LSEIK). Furthermore, the available forecasts nicely fits our interest in sea ice prediction up to 2 weeks. We used the daily 24-h atmospheric forecasts over the period of June 1st – August 31st and five 15-day forecasts initialized on five different dates (June 16th, July 1st, July 16th, August 1st and August 16th, 2010) at 00 UTC.

Each of the selected UKMO ensemble forecasts consists of one unperturbed 'control' forecast and 23 forecasts with perturbed initial conditions. The forcing variables used by the ice-ocean model are given every 6 hours: 10-m surface winds, 2-m air temperatures and specific humidity, precipitation as well as incoming long-wave and short-wave radiative fluxes. As there is no precipitation output at 00 UTC, the precipitation at 00 UTC is replaced with the forecasts at 06 UTC.

Following Parkinson and Washington (1979), the incoming short-wave radiation (Q) is obtained by applying the cloudiness factor (c) by Laevastu (1960) to global radiation under cloudless skies (Q_0)

$Q = Q_0(1 - 0.6c^3)$ (1)

Q_0 is calculated from an empirical equation by Zillman (1972)

$$Q_0 = \frac{S\cos^2 Z}{(\cos Z + 2.7)e \times 10^{-5} + 1.085\cos Z + 0.10} \quad (2)$$

S is the solar constant (1353W/m^2; Thekaekara and Drummond, 1971), the cosine of the zenith angle $\cos Z$ is caculated by the standard geometric formula

$\cos Z = \sin\emptyset \sin\delta + \cos\emptyset \cos\delta \cos HA$ (3)

where $\emptyset$, δ, and HA are latitude, declination, and hour angle, respectively (Sellers, 1965). The approximate δ and HA are determined as

$\delta = 23.44° \times \cos[(172 - day\ of\ year) \times \pi/180]$

$HA = (12\ hours - solar\ time) \times \pi/12$ (4)

while the vapor pressure e is calculated by an empirical formula of Murray (1967):

$e = 611 \times 10^{a(T_d - 273.15)/(T_d - b)}$ (5)

where T_d is the surface dew point temperature (in units of K), $(a, b) = (9.5, 7.66)$ for an ice cover and $(7.5, 35.86)$ for water surface. The cloudiness factor (c) and T_d are given by the UKMO data set.

The incoming long-wave radiation is estimated from Idso and Jackson's (1969) formula for clear skies and modified by a cloudiness factor of $(1 + cn)$

$$F\downarrow = \sigma {T_a}^4\{1 - 0.261\exp[-7.77 \times 10^{-4}(273 - T_a)^2]\} \times (1 + cn) \quad (6)$$

The Stefan-Boltzmann constant (σ) is $5.67 \times 10^{-8} Wm^{-2}K^{-4}$, T_a is the surface air temperature, c is the cloud cover value, and n is an empirical factor of 0.275 (Marshunova, 1966).

The specific humidity is calculated from

$$q = \frac{\varepsilon e}{p-(1-\varepsilon)e} \quad (7)$$

Where $\varepsilon = 0.622$ is the ratio of the molecular weight of water vapor to that of dry air (Hess, 1959), p is the surface air pressure, the vapor pressure e can be calculated from equation (5). The surface air pressure is given by the UKMO forcing data set.

2.3 Sea ice observation data

The sea ice concentration observations used in the assimilation are derived from DMSP F-17 SSMIS passive microwave data (Cavalieri et al., 2012; http://nsidc.org/data/docs/daac/nsidc0051_gsfc_seaice.gd.html). As independent information used for our system assessment we exploited the ice concentration data from the European Meteorological Satellite Agency (EUMETSAT) Ocean and Sea Ice Satellite Application Facility (OSISAF) (Eastwood et al., 2011; http://www.osi-saf.org). Notice, that the OSISAF concentration for the summer 2010 is derived from a different passive microwave sensor SSM/I onboard of DMSP F-15, so that it is an independent observation data.

As independent observational data for ice thickness we used measurements of sea ice draft from Beaufort Gyre Experiment Program (BGEP) Upward Looking Sonar (ULS) moorings located in the Beaufort Sea (http://www.whoi.edu/beaufortgyre) and sea ice thickness data obtained from autonomous ice mass-balance buoys (Perovich et al., 2009; http://IMB.crrel.usace.army.mil). The error in ULS measurements of ice draft is estimated as 0.1 m (Melling et al., 1995); drafts are converted to thickness by multiplying a factor of 1.1 (Nguyen et al., 2011). The accuracy of both IMB sounders is 5 mm (Richter-Menge et al., 2006). The location of the moorings BGEP_2009A, BGEP_2009D and the tracks of the ice mass-balance buoys IMB_2010A and IMB_2010B are shown in Figure 1.

2.4 Data assimilation

The data assimilation method we used in this study is similar to the one described by Yang et al. (2014). The satellite-derived sea ice concentrations are assimilated into the MITgcm using the sequential tracks of the SEIK filter with second-order exact sampling (Pham, 2001) as coded within the Parallel Data Assimilation Framework (PDAF, Nerger and Hiller, 2013, http://pdaf.awi.de). The SEIK filter is an ensemble-based Kalman filter method. The required initial ensemble, which represents the initial state estimate and the corresponding state error covariance matrix of the sea ice concentration and sea ice thickness, for simplicity, is generated from the daily snapshots of a model integration driven by the 24-h UKMO forecasts over the period of June 1st to August 31st, 2010. In a real application we would use a similar sampling

period from the previous model year, or maybe even averaged over many previous model years (Yang et al., 2014). The 92 state vectors are stored in a matrix, which is decomposed into Empirical Orthogonal Functions (EOFs). The leading 22 EOFs are transformed by the second-order exact sampling to generate the initial ensemble of ice concentration and thickness. During the assimilation experiments, the ensemble dynamically evolves in time, driven by atmospheric forcing, to produce a forecast ensemble. Every 24 hours, the ensemble forecast is combined with the observations to create an analysis ensemble that is used to initialize a new forecast ensemble. The corrections are based on model-data misfit with the error statistics assuming Gaussian error distributions. After the analysis step, the next forecast is computed by propagating the analysis ensemble with the model. To match with the ensemble size of the UKMO perturbed forcing, 23 ensemble states are used in this study. The SEIK analysis is applied locally at each model grid point with observations used within a radius of 126 km (~7 grid points). To stabilize the assimilation procedure and to account for model error the forecast covariance matrix can be inflated by the so-called "forgetting factor" (Pham, 2001). For more details on the localized SEIK filter and its implementation, the reader is referred to Nerger et al. (2006), Janjić et al. (2011) and Losa et al. (2012).

2.5 Experiment design and error statistics

The skill of the sea ice analysis and forecasts are validated with a series of 24 h forecasts in which LSEIK filter is applied every day at 00 UTC over the period of June 1st to August 30th, 2010. On five different days (June 16th, July 1st, July 16th, August 1st and August 16th, 2010), forecasts up to 15 days are started and also evaluated. The real-time ensemble atmospheric forecasts and the near-real time sea ice concentration data mimic a real forecasting experiment except that it is performed with historical data to avoid data stream issues. The following two main ensemble-forecasting experiments only differ in the approximation of the forecast error covariance:

1. LSEIK-1: Forecasts initialized from analyses obtained by assimilating daily NSIDC SSMIS sea ice concentration data and using UKMO control forecasts as forcing. A forgetting factor of 0.99 is applied to inflate the ensemble.
2. LSEIK-2: Same as LSEIK-1, but the UKMO ensemble forecasts are used as the forcing for data assimilation. No ensemble inflation is applied.

To show the sensitivities of sea ice prediction to the atmospheric forcing forecast, we also carried out the following ensemble-forecasting experiment:

3. LSEIK-3: Forecasts up to 15 days based on the LSEIK-1 model states but with ensemble forcing.

Before performing the aforementioned experiments, we carried out a series of sensitivity experiments to calibrate the LSEIK systems. As described in Yang et al. (2014), we have tested several values of the observation error of sea-ice concentration (σ_{SIC}), localization radius, and the inflation of the forecast error statistics. With an observation error of $\sigma_{SIC} = 0.25$ the best agreement of the forecast with observations was obtained in both the LSEIK-1 and LSEIK-2 systems with respect to improvement of the forecast agreement with observations. A forgetting factor of 0.99 is used to inflate the forecast error covariance in the LSEIK-1 experiment. In case of the experiment

LSEIK-2 no inflation is applied, because model uncertainty is explicitly considered by the atmospheric ensemble forcing.

For the observation error one has to keep in mind that it does not only represent measurement error, but also a representation error, which is associated, for example, with the finite resolution of the model. On average the uncertainty in the observed sea ice concentrations amounts to about 10%. However, the errors of satellite-derived sea ice concentration are far larger in summer than in winter (Comiso and others, 1997). Overall, the "observation errors" used in the DA algorithms are linked to model uncertainties, representation errors, and the DA algorithm itself (Kivman et al., 2001). Accordingly, one has to consider the observation errors in this conditional context (Losa et al., 2012), which allows us to use them as a tuning parameter when setting up the data assimilation system.

3. Results

3.1. 24-h forecasts of sea ice concentration

Figure 2 compares the temporal evolution of the RMSE of ice concentration forecasts with and without data assimilation with respect to the assimilated NSIDC SSMIS data (Figure 2a), and the independent OSISAF concentration (Figure 2b) for June 1st to August 30th, 2010. We follow Lisæter et al. (2003) and Yang et al. (2014) and evaluate RMSE only at grid points where either the model or the observations have ice concentrations larger than 0.05. This makes the interpretation of the results easier by avoiding large errors where concentrations are very small.

Both data assimilation experiments (LSEIK-1 and LSEIK-2) reduce the deviations of the 24-h ice concentration forecasts from the satellite-based concentrations substantially when compared to the MITgcm forecasts without assimilation. The mean RMSE of the free-running model, LSEIK-1 and LSEIK-2 ensemble forecasts compared with NSIDC amount to 0.25, 0.13, and 0.11, respectively. For the independent OSISAF data, the RMSE amount to 0.25, 0.15 and 0.14, respectively. For the entire study period, the LSEIK-2 concentrations are closer to both the NSIDC and OSISAF observations than the LSEIK-1 concentrations. The difference grows over the simulation period and is largest in August. Thus, both ensemble-forecasting systems can improve the forecasts of sea ice concentration by assimilating the sea ice concentration observations. However, the improvement is larger when uncertainty in atmospheric forcing is taken into account in data assimilation.

3.2. 24-h forecasts of sea ice thickness

Figure 3 compares the model mean ice thickness from 24-h ensemble forecast with in-situ ULS-observations (BGEP_2009A, Figure 3a, and BGEP_2009D, Figure 3b). Note, that the numerical model carries mean thickness (volume over area) as a variable. The observed thickness is multiplied by NSIDC local ice concentration to arrive at the observed mean thickness shown in Fig. 3. Both forecasts with data assimilation (LSEIK-1 and LSEIK-2) show improvements over the MITgcm forecast without DA. While the free-running MITgcm forecast shows only a small decline in ice thickness, the thickness in both forecasts from assimilated states is more strongly reduced. At BGEP_2009A and BGEP_2009D, the thickness forecasts from the assimilation experiments are generally consistent with the measurements in July and August. Over the whole

period, the RMSEs at BGEP_2009A are reduced from 0.77m to 0.27m in LSEIK-1 and 0.28m in LSEIK-2. At BGEP_2009D the RMSEs are reduced from 0.97m to 0.46m in LSEIK-1 and 0.49m in LSEIK-2 24-h forecasts.

The IMB_2010A (Figure 3c) buoy passes through the polar data gap around the North Pole and so a constant sea ice concentration of 1.0 is simply assumed in calculating the mean thickness from observations. All 24-h forecasts are very close to each other and capture the observed downward trend. The RMSEs at IMB_2010A are 0.42m in model free-run, 0.44m in both LSEIK-1 and LSEIK-2. There, the assimilation cannot improve the fit over the free-running model. Because the IMB_2010A buoy passes through the polar data gap around the North Pole during this summer period, and no valid observation can be used in the assimilation (Yang et al., 2014). Consequently, the effects of assimilating concentration far away from this buoy has little effect.

The ice thickness at IMB_2010B (Figure 3d) has only 10 data points in the period of June 6th to August 8th, because its snow sounder failed on May 7th. Similar to IMB_2010A, all the 24-h forecasts have a positive bias of about 1.0 m on June 6th. However, the LSEIK-1 and LSEIK-2 forecasts capture the downward trend after July 11st better than the free-running model. The RMSEs at IMB_2010B are reduced from 0.90m to 0.59m with LSEIK-1 to 0.60m with LSEIK-2.

3.3. 15-day forecasts of sea ice concentration and thickness

Besides the 24-h forecasts during the assimilation procedure, we computed forecasts for up to 15 days that are initialized on 5 different dates. Each of these medium-range forecasts is forced by 15-day atmospheric forecasts. The RMSEs of ice concentration for these medium-range forecasts are shown in Figure 2. The 15-day forecasts for LSEIK-1 and LSEIK-2 show a rapid increase of RMSEs with forecast lead-time. Such an increase is expected, as forecast error for atmospheric fields grow rapidly within the 15-day forecast period. However, the RMSEs from both LSEIK-1 and LSEIK-2 are always lower than the errors of the 24-h forecasts without DA. As the error of the initial states are lower for LSEIK-2 than LSEIK-1, the forecasts from LSEIK-2 show the smallest errors.

The 15-day sea ice thickness forecasts at BGEP_2009A and BGEP_2009D are shown in Figure 5a and 5b. Similar to the 24-h forecasts, the ice thickness improvements in LSEIK-1 and LSEIK-2 are small for the forecast initialized on June 16th. This is because the differences in the initialized thickness between the forecasts with and without assimilation are small. As the initialized ice thickness is more realistic, the forecast improvements over the 24-h free-running model forecasts are larger in July and August. Both LSEIK-1 and LSEIK-2 15-day forecasts capture the observed trend of decreasing thickness.

By replacing the single control forcing with the ensemble forcing, we examine the impacts of ensemble forcing on the sea ice concentration and thickness forecasts. Based on the initialization from LSEIK-1, but with ensemble forcing, the case LSEIK-3 shows smaller RMSEs than LSEIK-1, and their differences become larger with forecast lead time. The bias of the deterministic forecast appears to be reduced by using an ensemble forcing.

The medium-range sea ice thickness forecasts using control forcing and ensemble forcing are also compared in Figure 3. In the first few forecast days, the differences between LSEIK-1 and LSEIK-3 are quite small, and their differences become larger with longer forecast lead times. This difference, however, is still within the range of observed ice thickness uncertainty.

4. Discussion

In the previous section, we saw that by using an ensemble forcing data assimilation analyses and medium-range forecasts of sea ice can be improved when compared to using a single deterministic control forcing. Here, we examine the reasons for this effect from the perspective of the ensemble spread and cross-correlations.

4.1 Sea ice concentration and thickness ensemble spread

In Figure 4a, we show the evolution of spatially averaged sea ice concentration spread measured by the ensemble standard deviations (STDs) of the 24-h forecasts discussed in section 3.1. As for the RMSEs, the spread is computed only at grid points where either the modelled or observed ice concentrations are larger than 0.05. Both, LSEIK-1 and LSEIK-2 have an initial mean STD of about 0.05. Over time, the STD decreases gradually because of the data assimilation of every 24 h. As the ice melting is a more important contributor to ice concentration variance in late summer (Lisæter et al., 2003), the spread finally increases slightly with summer melting in both LSEIK-1 and LSEIK-2. During most of the time, the spatially averaged spread of the LSEIK-2 24-h forecasts of sea ice concentration is slightly larger than the LSEIK-1 forecasts. Averaged over the 3-month period the STDs are 0.03 for LSEIK-2 and 0.02 for LSEIK-1. The size of the ensemble spread is also indicated by the shaded colors in Figure 2. This shows that the estimated uncertainty in ice concentration forecasts implied by the ensemble is significant.

Figure 5 shows the spatial distributions of the ensemble spread of 24-h ice concentration forecasts from LSEIK-1 and LSEIK-2 on June 10th and August 30th, 2010. Both, LSEIK-1 and LSEIK-2 ensemble forecasts have similar spread distribution patterns at both dates. The highest STDs are mainly found close to the data void North Pole and the sea ice edge area (e.g. the East Siberian Sea, Canadian Basin, Beaufort Sea, and Greenland Sea). As assimilation updates of the sea ice concentration can only happen when the ensemble spread is non-zero, the maps show that updates mainly occur in the sea ice edge area, and the updates in the central area, where multi-year sea ice prevails, is very small. For August 30th, the STDs outside the peaks are slightly larger for LSEIK-2 than for LSEIK-1. This is consistent with the larger mean ensemble spread shown in Figure 4a, and further shows that the size of prior error covariance as a measure of model uncertainty is larger in LSEIK-2, thus more weight is given to data and less weight to the model prior in the analysis step, accordingly, LSEIK-2 is more closer fit to observations which is visible in Figure 3.

The evolution of spatially averaged ensemble STDs of sea ice thickness is shown in Figure 4b. Both LSEIK-1 and LSEIK-2 have an initial STD of about 0.20m. Over time, the spread again decreases with data assimilation. The spread is generally smaller for LSEIK-2 than LSEIK-1. During August, the difference is about 0.02m. The shaded colors in Figure 3 also show the

ensemble spread at BGEP_2009A and BGEP_2009D highlighting the fact that ice thickness spread is small compared to the thickness.

The spatial distribution of ice-thickness STDs from LSEIK-1 and LSEIK-2 are shown in Figure 6 for June 10th and August 30th, 2010. On June 10th, the high STDs are mainly found in data void areas close to the North Pole, the multi-year sea ice region north of Greenland and the Canadian Archipelago, as well as the sea ice edge area (e.g., East Siberian Sea, Chukchi Sea, Canadian Basin , Beaufort Sea). On August 30th, the high STDs are mainly in the North Pole data gap area and in the multi-year sea ice area. The spread in the north of Greenland and the Canadian Archipelago and in Beaufort Sea is larger at end of August in LSEIK-1 (Figure 6b) than that in LSEIK-2 24-h forecasts (Figure 6d). This larger spread might actually be a spurious effect of the inflation by the forgetting factor. Because from Figure 5, the STD of ice concentration is low in this region, so that prior errors are small and the analysis update is small and the ensemble variance is only slightly reduced. However, the inflation is applied uniformly over the whole assimilation domain and for both the ice concentration and the thickness. Accordingly, the ensemble spread in LSEIK-1 might grow unrealistically over time in this region.

For the 15-day forecasts, Figure 4 shows that the ensemble spreads grow faster when the ensemble forcing is applied than with the single control forcing of LSEIK-1. This more rapid increasing spread helps improve the 15-day forecasts of LSEIK-2 by accounting more realistically for the model uncertainties.

4.2 Sea ice concentration and thickness ensemble cross-correlations

As only observations of sea ice concentrations are assimilated, the ice thickness is influenced by the data assimilation only through the covariances between the point-wise ice concentration and thickness. To examine the differences in LSEIK-1 and LSEIK-2, we show in Figure 7 time-distance plots of the point wise grid-cell correlations between the 24-h forecasts of ice concentration and ice thickness in LSEIK-1 and LSEIK-2.

The distance indicates here the location along section AB shown in Figure 1. This particular section in the Beaufort Sea is chosen to explain the sea ice thickness evolution in the region near BGEP_2009A and BGEP_2009D. The section crosses the location of BGEP_2009A half way at 270 km, while BGEP_2009D is close to the end of the section at 540 km. At the end of the experiments, the ice disappeared at some grid points in all ensemble members. These occurrences are shown as white boxes.

The correlations between ice concentration and ice thickness in LSEIK-1 and LSEIK-2 have similar distributions and vary similarly over time. Both reveal a mostly positive correlation between ice concentration and ice thickness. This is consistent with Lisæter et al. (2003), and can be explained by sea ice thermodynamics of reducing horizontal melting for thicker ice. The quite few negative correlations are probably refered to the sea ice dynamics of divergence in the Beaufort Gyre area.

Initially, the ice concentrations in the model and the observations are very close to one, along the

section. At this time, the assimilation has only a very small influence. Hence, also the ice thickness is only slightly changed despite the large correlation between ice concentration and thickness. The situation changes after about June 21st. At this time, the measured concentrations have decreased to about 0.7, while the forecasted concentration in LSEIK-1 and LSEIK-2 are still at about 0.8. Hence, the assimilation reduces the concentrations. The effect on the thickness depends again on the estimated cross-correlations between the ice concentration and thickness.

At the location of BGEP_2009A (distance=270km along the section), the cross-correlation for both LSEIK-1 and LSEIK-2 is above 0.6 during most of the summer period, this can explain the good sea-ice thickness agreements with the observations as shown in Figure 3a. We also note the cross-correlation is almost zero near July 31st in LSEIK-1, this results in the under-estimation in LSEIK-1. The mooring BGEP_2009D is close to the end of the section at 540km. Here, the cross-correlations in LSEIK-1 and LSEIK-2 are very low in most of June and explains why the improvement is very small in both experiments with DA. In July, the cross-correlation becomes much larger, and both LSEIK-1 and LSEIK-2 capture the thickness decrease as shown in Figure 3b. Note the correlation from July 20th to August 8th in LSEIK-2 is only from 0 to 0.20, in contrast, the correlation in LSEIK-1 is as high as 0.60. This fact is consistent with the better agreements in thickness in LSEIK-1 and the over-estimated thickness in LSEIK-2 during this period (Figure 3b).

5. Summary and conclusion

This article presents a case study using UKMO ensemble atmospheric forecasts from the TIGGE archive for Arctic sea ice forecasts with a sea ice-ocean model. To study the value of using the TIGGE database in the Arctic summer sea ice forecasts, we carry out two kinds of ensemble forecasts. Both forecasts assimilate the satellite-based sea ice concentration data with an LSEIK filter but with different configuration and forcing. The first one (LSEIK-1) is driven by the deterministic control forcing and uses a forgetting factor to artificially inflate the ensemble error covariances, while the second (LSEIK-2) is forced by UKMO ensemble atmospheric forecasts during the data assimilation cycle. The results show that both systems largely improve the analyses and 24-h forecasts of sea ice concentration. Furthermore, sea ice concentration forecasts based on LSEIK-2 show smaller errors than those based on LSEIK-1. Compared with the MITgcm forecast without DA, both LSEIK systems improve the analyzed and 24-h sea ice thickness forecasts in late July and August, but the improvements in June are small. The strong positive ice concentration-thickness correlations contribute to the ice thickness forecasting improvement after July.

Furthermore, in these experiments we find that the configuration of the LSEIK-2 system is significantly easier to implement than the LSEIK-1 system. As discussed in Yang et al. (2014), we had to carry out a large effort to tune the LSEIK-1 forecasting system. It involved a series of sensitivity experiments with different values of sea ice concentration data uncertainties, localization radius, and forgetting factor to inflate the forecast error statistics. As model errors are already explicitly accounted for by the ensemble forcing, there is no need to use a forgetting factor in the LSEIK-2 system. So it is more convenient to implement than the LSEIK-1 system.

Besides the improvement in the data assimilation system, the impacts of ensemble forcing on 15-day forecasts of sea ice concentration and thickness are also examined by comparing forecasts from the same initialized model states but with different forcing. It shows that by considering the model uncertainties, the ensemble mean forecasts of sea ice concentration can be improved with ensemble forcing, and the improvement grows with the forecast lead time. The ice thickness differences also become larger with longer forecast lead times but still remain within the observation uncertainties, so the improvement in the ice thickness forecasts is evaluated to be not significant.

To our knowledge this is the first study in which true ensemble forcing data in the Arctic sea ice forecasts are used. We find that with the ensemble forcing data, the initialization and forecast quality can be potentially improved and forecast lead times can be extended. This promises benefits for the quality of Arctic sea ice forecasts and hence their usability for marine activities. Further, previous studies have already shown that using multi-model ensembles can further improve the atmospheric forecasts than the single model ensembles (Bougeault et al., 2010). We plan to examine Arctic sea ice forecasts using TIGGE multi-model ensembles in the future work.

Acknowledgements
The UKMO ensemble forecasting data were accessed through the TIGGE data server in European Centre for Medium-Range Weather Forecasts (ECWMF). We thank the National Snow and Ice Data Center (NSIDC) and the OSISAF High Latitude Processing Centre for providing the ice concentration data, the Woods Hole Oceanographic Institution for sea ice draft data, and the Cold Regions Research and Engineering Laboratory or IMB data. This study was supported by the BMBF (Federal Ministry of Education and Research, Germany) - SOA (State Oceanic Administration, China) Joint Project (01DO14002), the National Natural Science Foundation of China (41376005 and 41376188), the Ocean Public Welfare Project of China (2012418007) and the China Scholarship Council.

References

Bishop CH, Etherton BJ, Majumdar SJ. 2001. Adaptive sampling with the ensemble transform Kalman filter. Part I: Theoretical aspects. Mon. Weather Rev. 129: 420–436.

Bougeault P, and Coauthors. 2010. The THORPEX Interactive Grand Global Ensemble. Bull.Amer. Meteor. Soc. 91:1059–1072.

Bowler NE, Arribas A, Mylne KR, Robertson KB. 2007. 'The MOGREPS short-range ensemble prediction system. Part I: System description.' Met Office NWP Technical Report No. 497, pp. 18. Available from The Met Office, FitzRoy Rd, Exeter, EX1 3PB, UK (see also UKMO web page).

Buehner M, Caya A, Carrieres T, Pogson L, Lajoie M. 2013. Overview of sea ice data assimilation activities at Environment Canada. In Proceedings of the ECMWF-WWRP/THORPEXWorkshop on Polar Prediction, 24–27 June, 2013. ECMWF: Reading, UK.

Cavalieri DJ, Parkinson CL, DiGirolamo N, Ivanoff A. 2012. Intersensor calibration between F13 SSMI and F17 SSMIS for global sea ice data records. IEEE Trans. Geosci. Remote Sens. 9(2): 233-236.

Comiso JC, Cavalieri DJ, Parkinson CL and Gloersen P. 1997. Passive microwave algorithms for sea ice concentration: A comparison of two techniques. Remote. Sens. Environ. 60(3): 357-384.

Eastwood S, Larsen KR, Lavergne T, Neilsen E, Tonboe R. 2011. OSI SAF global sea ice concentration reprocessing: product user manual, version 1.3. EUMETSAT OSI SAF (Product 0SI-409).

Eicken H. 2013. Ocean science: Arctic sea ice needs better forecasts, Nature, 497(7450): 431-433.

Hess SL. 1959. Introduction to Theoretical Meteorology, 362 pp., Holt, Rinehart, and Winston, New York.

Idso SB and Jackson RD. 1969. Thermal radiation from the atmosphere. J. Geophys. Res., 74: 5397-5403.

IPCC. 2013. Climate Change 2013: The Physical Science Basis. Contribution of Working Group I to the Fifth Assessment Report of the Intergovernmental Panel on Climate Change [Stocker T F, Qin D, Plattner G K, et al. (eds.)]. Cambridge University Press, Cambridge, United Kingdom and New York, NY, USA, 1535 pp.

Janjić T, Nerger L, Albertella A, Schröter J, Skachko S. 2011. On domain localization inensemble based Kalman filter algorithms. Mon. Wea. Rev., 139: 2046–2060.

Jung T, Leutbecher M. 2007: Performance of the ECMWF forecasting system in the Arctic during winter. Quart. J. Roy. Meteor. Soc., 133, 1327-1340.

Kivman G A, Kurapov A L, Guessen A. 2001. An entropy approach to tuning weights and smoothing in the generalized inversion. J. Atmos. Oceanic Technol., 18, 266–276.

Laevastu T. 1960. Factors affecting the temperature of the surface layer of the sea. Comment. Phys. Math., 25:1.

Lindsay RW, Zhang J. 2006. Assimilation of ice concentration in an ice-ocean model. J. Atmos. Oceanic Technol., 23(5): 742-749.

Lisæter KA, Rosanova J, Evensen G. 2003. Assimilation of ice concentration in a coupled ice–ocean model, using the Ensemble Kalman filter, Ocean Dyn., 53(4): 368-388.

Liu J, Song M, Horton RM, Hu Y. 2013. Reducing spread in climate model projections of a September ice-free Arctic. Proc. Natl. Acad. Sci. U.S.A., 110(31): 12571-12576.

Losa S, Danilov S, Schröter J, Nerger L, Maßmann S, and Janssen F. 2012. Assimilating NOAA SST data into the BSH operational circulation model for the North and Baltic Seas: Inference about the data, J Marine. Syst., 105-08: 152-162.

Losch M, Menemenlis D, Campin JM, Heimbach P and Hill C. 2010.On the formulation of sea-ice models. Part 1: Effects of different solver implementations and parameterizations, Ocean Modell., 33(1): 129-144.

Marshall J, Adcroft A, Hill C, Perelman L and Heisey C. 1997. A finite-volume, incompressible Navier Stokes model for studies of the ocean on parallel computers, J. Geophys. Res., 102(C3), 5753-5766.

Marshunova, MS. 1966. Principal characteristics of the radiation balance of the underlying surface and of the atmosphere in the Arctic, in Soviet Data on the Arctic Heat Budget and Its Climatic Influence, edited by J. O. Fletcher, B. Keller, and S. M. Olenicoff, pp. 51-131, Rand Corporation, Santa Monica, Calif.

Menemenlis D, Campin J-M, Heimbach P, Hill C, Lee T, Nguyen A, Schodlok M and Zhang H. 2008. ECCO2: High resolution global ocean and sea ice data synthesis, Mercator Ocean Q. Newsl., 31: 13-21.

Murray FW. 1967. On the computation of saturation vapor pressure. J. Appl. Meteorol., 6: 203-204.

Nguyen AT, Menemenlis D, Kwok R. 2011. Arctic ice-ocean simulation with optimized model parameters: Approach and assessment, J. Geophys. Res., 116(C4): C04025, doi:10.1029/2010JC006573.

Melling H, Johnston PH, Riedel DA. 1995. Measurements of the underside topography of sea ice by moored subsea sonar, J. Atmos. Oceanic Technol., 12(3): 589-602.

Nerger L, Danilov S, Hiller W, Schröter J. 2006. Using sea-level data to constrain a finite-element primitive-equation ocean model with a local SEIK filter, Ocean Dyn., 56(5-6): 634-649.

Nerger L, Hiller W. 2013. Software for ensemble-based data assimilation systems—Implementation strategies and scalability, Comp. & Geosci., 55: 110-118.

Park Y-Y, Buizza R, Leutbecher M. 2008. TIGGE: preliminary results on comparing and combining ensembles. Quart. J. Roy. Meteor. Soc., 134: 2029–2050.

Parkinson CL, Washington WM. 1979. A large-scale numerical model of sea ice, J. Geophys. Res., 84(C1): 311–337, doi:10.1029/JC084iC01p00311.

Perovich DK, Richter-Menge JA, Elder B, Claffey K, Polashenski C. 2009. Observing and understanding climate change: Monitoring the mass balance, motion, and thickness of Arctic sea ice, http://imb.crrel.usace.army.mil/.

Pham DT, Verron J, Gourdeau L. 1998. Singular evolutive Kalman filters for data assimilation in oceanography, C. R. Acad. Sci. Paris, Earth Planet. Sci. , 326: 255-260.

Pham DT. 2001. Stochastic methods for sequential data assimilation in strongly nonlinear systems. Mon. Wea. Rev., 129(5): 1194-1207.

Richter-Menge JA, Perovich DK, Elder BC, Claffey K, Rigor I, Ortmeyer M. 2006. Ice mass-balance buoys: a tool for measuring and attributing changes in the thickness of the Arctic sea-ice cover, Ann. Glaciol., 44(1): 205-210.

Sakov P, Counillon F, Bertino L, Oke PR, Korablev A. 2012. TOPAZ4: an ocean-sea ice data assimilation system for the North Atlantic and Arctic. Ocean Sci, 8: 633–656.

Sellers WD. 1965. Physica Cllimatology 272 pp., University of Chicago Press, Chicago, Ill.

Shutts G. 2005. A kinetic energy backscatter algorithm for use in ensemble prediction systems. Q. J. R. Meteorol. Soc. 131: 3079–3102.

Smith W H, and Sandwell D T. 1997. Global sea floor topography from satellite altimetry and ship depth soundings, Science, 277(5334): 1956-1962.

Stark JD, Ridley J, Martin M, Hines A. 2008. Sea ice concentration and motion assimilation in a sea ice−ocean model. J. Geophys. Res., 113(C5): C05S91, doi:10.1029/2007JC004224.

Thekaekara MP, Drummond AJ. 1971. Standard values for the solar constant and its spectral components. Nature Phys. Sci., 229: 6-9.

Tietsche S, Notz D, Jungclaus J, Marotzke J. 2013. Assimilation of sea-ice concentration in a global climate model- physical and statistical aspects. Ocean Sci., 9(1): 19-36.

Yang Q, Losa NS, Losch M, Liu J, Zhang Z, Nerger L and Yang H. 2014. Assimilating summer sea ice concentration into a coupled ice-ocean model using a localized SEIK filter, Ann. Glaciol., 56(69), doi: 10.3189/2015AoG69A740.

Zhang J and W Hibler III. 1997. On an efficient numerical method for modeling sea ice dynamics, J. Geophys. Res., 102(C4): 8691-8702.

Zillman JW. 1972. A study of some aspects of the radiation and heat. 337pp., Bur. of Meteorol., Dep. of the Interior, Canberra, Australia.

Figure Captions

Figure 1. Locations of sea ice thickness observation and buoy trajectories from June 1st to August 30th, 2010. BGEP_2009A (magenta square), BGEP_2009D (red square), IMB_2010A (blue line) and IMB_2010B (green line). A section used in the text (section AB; start from A) is shown as a black line (updated from Yang et al., 2014).

Figure 2.Temporal evolution of RMSE differences between sea ice concentration forecasts and (a) NSIDC SSMIS and (b) OSIAF ice concentration data. The RMSE of the MITgcm free-run, LSEIK-1 and LSEIK-2 24-h forecasts are shown as gray, blue and red solid lines, respectively. The LSEIK-1 and LSEIK-2 15-day forecasts initialized on June 16th, July 1st, July 16th, August 1st and August 16th, 2010 are shown as blue and red dashed lines. The spread (STDs) of the LSEIK-2 and LSEIK-3 15-day ensemble forecasts initialized on August 16th, 2010 are also shown with blue and red shaded colors.

Figure3. Evolution of mean sea ice thickness (m) at (a) BGEP_2009A, (b) BGEP_2009D Beaufort Sea, (c) IMB_2010A and (d) IMB_2010B from June 1st to August 30th, 2010. The black solid lines show the obtained mean ice thickness observations. The MITgcm free-run, LSEIK-1 and LSEIK-2 24-h thickness forecasts are shown as gray, blue and red solid lines. The LSEIK-1 and LSEIK-2 15-day forecasts initialized on June 16th, July 1st, July 16th, August 1st and August 16th, 2010 are shown as blue and red dashed lines. The spread (STDs) of the LSEIK-2 and LSEIK-3 15-day ensemble forecasts initialized on July 16th, 2010 are also shown with blue and red shaded colors.

Figure 4. Temporal evolution of area mean spread of (a) ice concentration and (b) ice thickness forecasts. The spread (STDs) of LSEIK-1 and LSEIK-2 24-h forecasts are shown as blue and red solid lines. The spread (STDs) of LSEIK-1, LSEIK-2 and LSEIK-3 15-day forecasts initialized on June 16th, July 1st, July 16th, August 1st and August 16th, 2010 are shown as blue, green and red dashed lines.

Figure 5. Sea ice-concentration standard deviation for the individual grid cells as calculated from the LSEIK-1 (top) and LSEIK-2 (bottom) 24-h ensemble forecasts, on June 10th (left) and August 30th (right), 2010.

Figure 6. Sea ice-thickness standard deviation for the individual grid cells as calculated from the LSEIK-1 (top) and LSEIK-2 (bottom) 24h ensemble forecasts, on June 10th (left) and August 30th (right), 2010.

Figure 7. Time/distance plots for the grid-cell ensemble based correlation between ice concentration and ice thickness along section AB in Figure 1, (a) LSEIK-1 forecast, (b) LSEIK-2 forecast. The section AB crosses the location of BGEP_2009A half way at 270 km (middle of the figure, marked in black triangle), while BGEP_2009D is close to the end of the section at 540 km (bottom of the figure, marked in black quare).

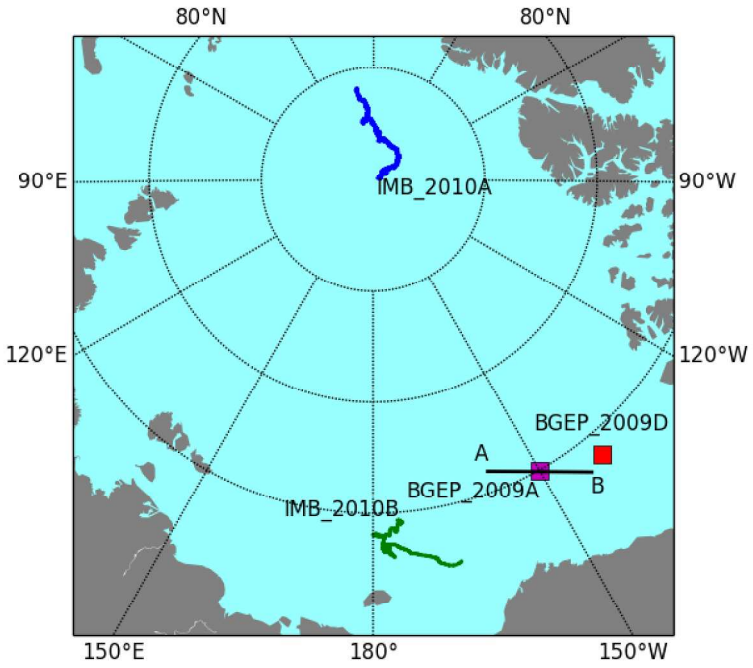

Figure 1. Locations of sea ice thickness observation and buoy trajectories from June 1st to August 30th, 2010. BGEP_2009A (magenta square), BGEP_2009D (red square), IMB_2010A (blue line) and IMB_2010B (green line). A section used in the text (section AB; start from A) is shown as a black line (updated from Yang et al., 2014).
203x152mm (300 x 300 DPI)

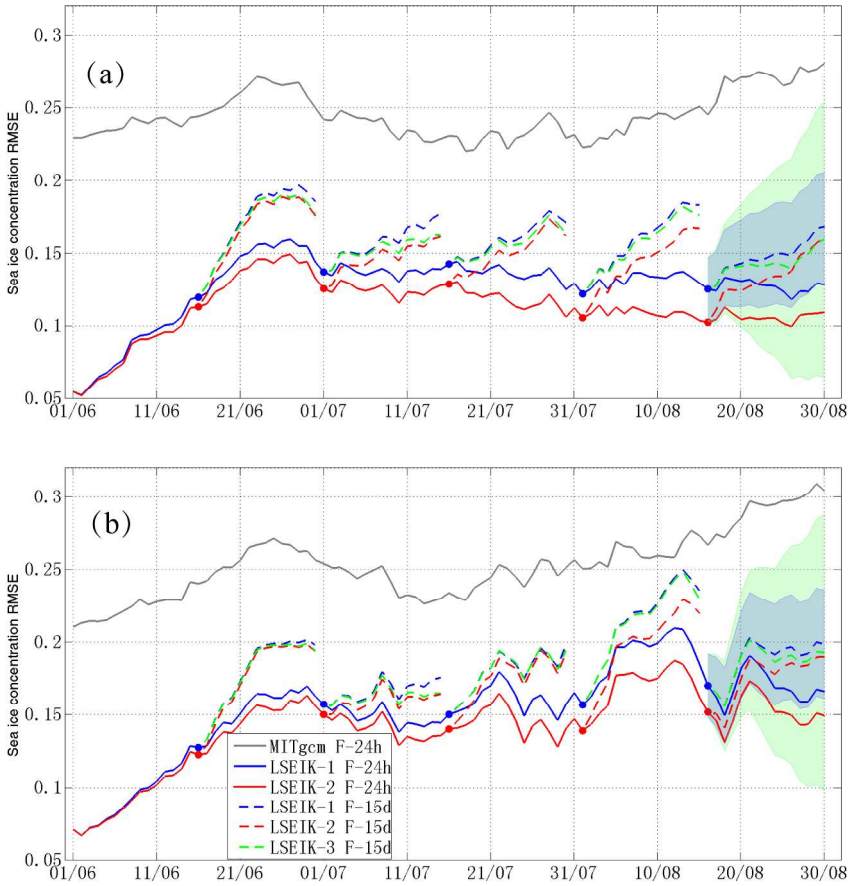

Figure 2.Temporal evolution of RMSE differences between sea ice concentration forecasts and (a) NSIDC SSMIS and (b) OSIAF ice concentration data. The RMSE of the MITgcm free-run, LSEIK-1 and LSEIK-2 24-h forecasts are shown as gray, blue and red solid lines, respectively. The LSEIK-1 and LSEIK-2 15-day forecasts initialized on June 16th, July 1st, July 16th, August 1st and August 16th, 2010 are shown as blue and red dashed lines. The spread (STDs) of the LSEIK-2 and LSEIK-3 15-day ensemble forecasts initialized on August 16th, 2010 are also shown with blue and red shaded colors.
209x197mm (300 x 300 DPI)

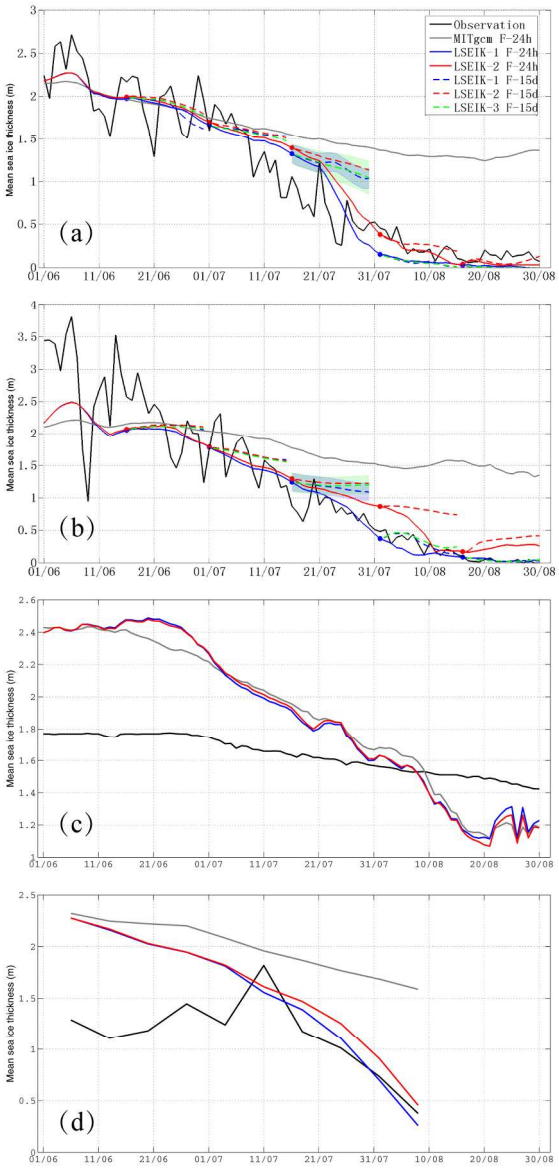

Figure3. Evolution of mean sea ice thickness (m) at (a) BGEP_2009A, (b) BGEP_2009D Beaufort Sea, (c) IMB_2010A and (d) IMB_2010B from June 1st to August 30th, 2010. The black solid lines show the obtained mean ice thickness observations. The MITgcm free-run, LSEIK-1 and LSEIK-2 24-h thickness forecasts are shown as gray, blue and red solid lines. The LSEIK-1 and LSEIK-2 15-day forecasts initialized on June 16th, July 1st, July 16th, August 1st and August 16th, 2010 are shown as blue and red dashed lines. The spread (STDs) of the LSEIK-2 and LSEIK-3 15-day ensemble forecasts initialized on July 16th, 2010 are also shown with blue and red shaded colors.
126x229mm (300 x 300 DPI)

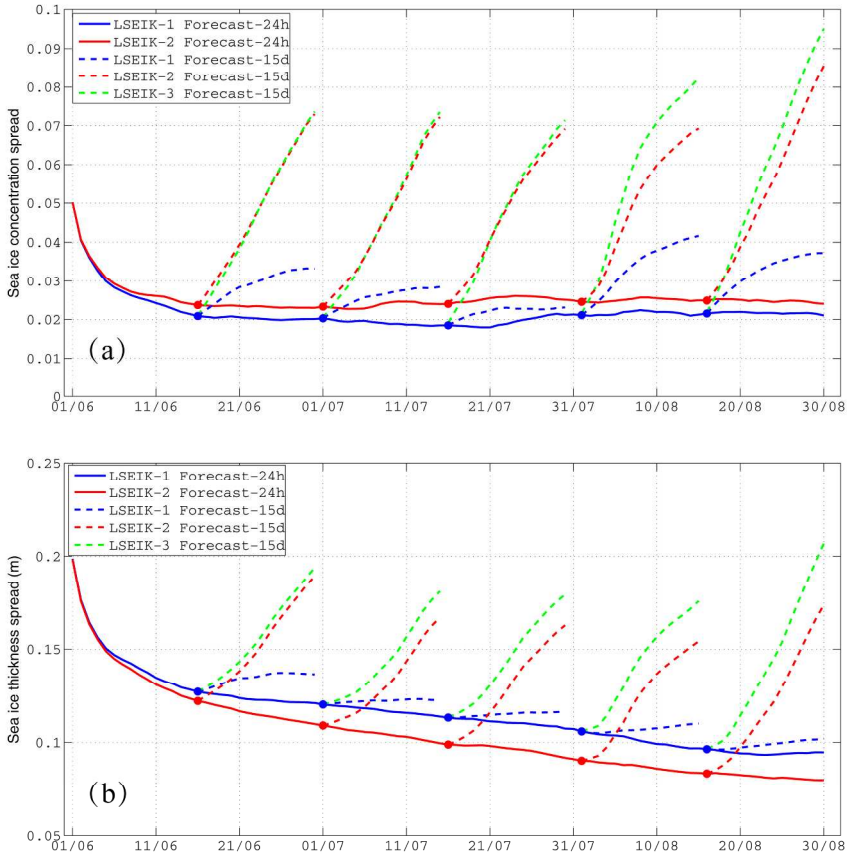

Figure 4. Temporal evolution of area mean spread of (a) ice concentration and (b) ice thickness forecasts. The spread (STDs) of LSEIK-1 and LSEIK-2 24-h forecasts are shown as blue and red solid lines. The spread (STDs) of LSEIK-1, LSEIK-2 and LSEIK-3 15-day forecasts initialized on June 16th, July 1st, July 16th, August 1st and August 16th, 2010 are shown as blue, green and red dashed lines.
217x198mm (300 x 300 DPI)

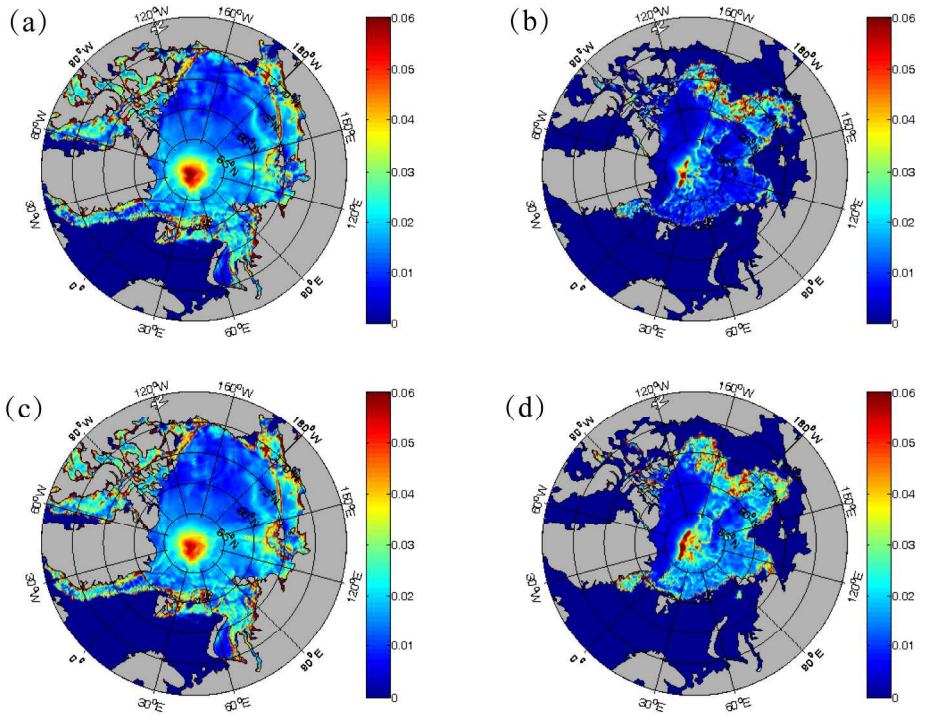

Figure 5. Sea ice-concentration standard deviation for the individual grid cells as calculated from the LSEIK-1 (top) and LSEIK-2 (bottom) 24-h ensemble forecasts, on June 10th (left) and August 30th (right), 2010. 213x160mm (300 x 300 DPI)

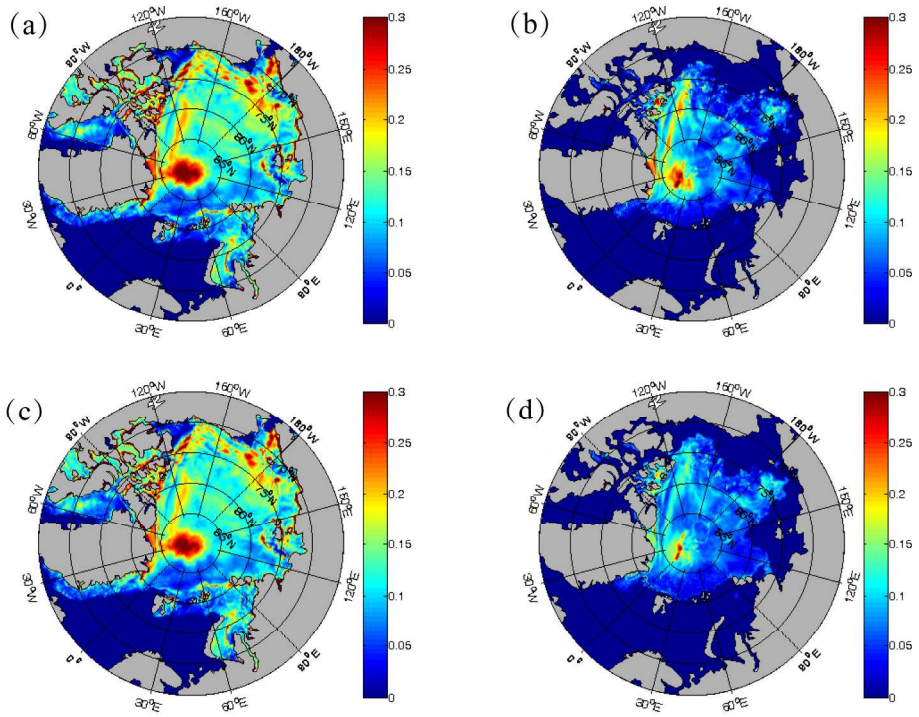

Figure 6. Sea ice-thickness standard deviation for the individual grid cells as calculated from the LSEIK-1 (top) and LSEIK-2 (bottom) 24h ensemble forecasts, on June 10th (left) and August 30th (right), 2010. 213x160mm (300 x 300 DPI)

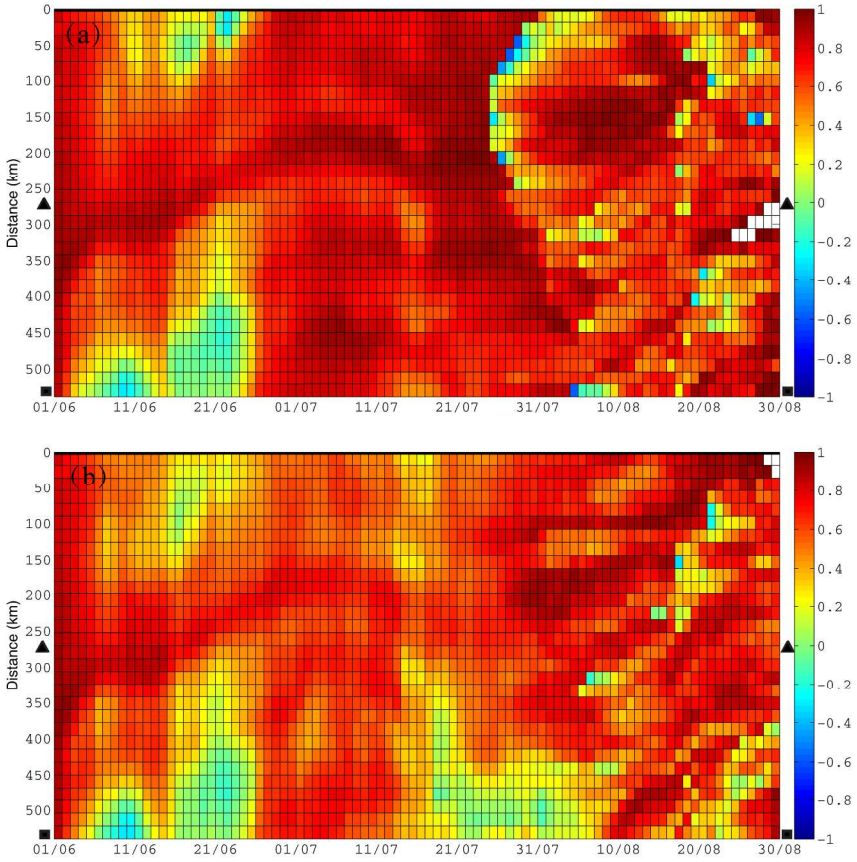

Figure 7. Time/distance plots for the grid-cell ensemble based correlation between ice concentration and ice thickness along section AB in Figure 1, (a) LSEIK-1 forecast, (b) LSEIK-2 forecast. The section AB crosses the location of BGEP_2009A half way at 270 km (middle of the figure, marked in black triangle), while BGEP_2009D is close to the end of the section at 540 km (bottom of the figure, marked in black quare). 231x212mm (300 x 300 DPI)